JOURNAL OF SYNCHROTRON RADIATION

ISSN 1600-5775

Received 31 October 2025
Accepted 23 February 2026

Edited by Y.-G. Lin, NSRRC, Taiwan

Keywords: X-ray Compton scattering; internal combustion engine; time-resolved technique; gas temperature.

Supporting information: this article has supporting information at journals.iucr.org/s

Imaging gas in a combustion engine with high-energy X-ray Compton scattering

Yuki Mizuno,[a] Hiroaki Suzuki,[b] Naruki Tsuji,[a]* Takuyo Oguchi,[a] Go Matsubara,[a] Hiroyuki Yamase[c]* and Yoshiharu Sakurai[a]

[a]Japan Synchrotron Radiation Research Institute, Sayo, Hyôgo 679-5198, Japan, [b]Japan AeroSpace Technology Foundation (JAST), Sendai, Miyagi 980-0811, Japan, and [c]Research Center of Materials Nanoarchitectonics (MANA), National Institute for Materials Science, Tsukuba, Ibaraki 305-0047, Japan. *Correspondence e-mail: ntsuji@spring8.or.jp, yamase.hiroyuki@nims.go.jp

We have developed a time-resolved Compton-scattering imaging technique for visualizing gas behaviours in operating internal combustion engines. This technique employs a digital processing system to record both the pulse height and the timing of detected X-rays, enabling the derivation of Compton-scattered X-ray spectra for each crank angle, which corresponds to the piston position. The observed crank-angle dependency of Compton-scattered X-ray intensity allowed us to successfully capture the density changes of the gas in the combustion chamber associated with piston motion and combustion. In addition, the capability of temperature estimation is discussed with a combination of X-ray Compton-scattering experiments and pressure measurements. This study demonstrates that time-resolved Compton-scattering imaging is a powerful and unique technique for characterizing gas behaviours in an operating internal combustion engine.

1. Introduction

For a more sustainable global environment, improving fuel efficiency and reducing exhaust gas emissions in internal combustion engines are essential. The combustion process in an engine cylinder is highly complex, governed by the dynamic distribution of fuel gas, combusted gas, temperature, ignition points and other factors. To better understand these intricate phenomena and enhance engine performance, direct in-cylinder visualization has been pursued using optically accessible engines (Bowditch, 1961; Zhao, 2012). These engines are equipped with optical windows that allow visible laser beams to be directed into the cylinder. However, the additional equipment and modifications required for optical access may influence the in-cylinder combustion process.

To overcome this limitation, we have been developing a time-resolved Compton-scattering imaging (CSI) technique for direct observation of in-cylinder gas behaviour. A key advantage of CSI over optical laser-based techniques is that it does not require any modifications to the engine. This is because CSI uses high-energy X-rays with high material transmittance, allowing penetration into the engine. Furthermore, even at high X-ray energies, Compton scattering exhibits a sufficient cross-section for light elements, making it suitable for visualizing in-cylinder gas behaviours.

Besides internal combustion engines, CSI has been applied as a visualization technique for investigating the behaviour of light-element materials inside palm-size energy devices. Using high-energy X-rays with high material transmittance, CSI has been used successfully to observe dynamic phenomena in

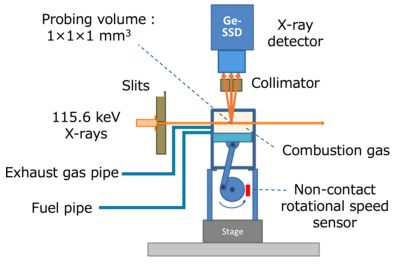

lithium-ion batteries and polymer electrolyte fuel cells. For example, migration of lithium in a commercial battery (Itou *et al.*, 2015; Suzuki *et al.*, 2020; Suzuki *et al.*, 2021) and the formation of liquid water in a fuel cell during operation (Tsuji *et al.*, 2021; Miyazawa *et al.*, 2023) have been clearly visualized using this method.

In a previous work on combustion gases, a self-sustaining flame made by a cylindrical Bunsen burner was measured using a scanning-type CSI technique (Sakurai *et al.*, 2016; Sakurai *et al.*, 2021). This result shows a large change in the intensity of Compton-scattered X-rays across the flame, due to variations in gas temperature. The intensity of Compton-scattered X-rays, dN, is given by

$$\mathrm{d}N = \Phi_0 t_1 t_2 \rho_\mathrm{e} \mathrm{d}V \frac{\mathrm{d}\sigma_\mathrm{KN}}{\mathrm{d}\Omega}, \quad (1)$$

where Φ_0 is the incident photon flux to the engine, t_1 is the incident X-ray transmittance to the probing volume, t_2 is the scattered X-ray transmittance from the probing volume to the X-ray detector, ρ_e is the average electron density over the probing volume dV and $\mathrm{d}\sigma_\mathrm{KN}/\mathrm{d}\Omega$ is the Klein–Nishina differential cross-section (Sharaf, 2001). Since t_1 and t_2 are assumed to be constant, the intensity of Compton-scattered X-rays, dN, probes the average electron density ρ_e. The ratio of molecular density to electron density, α, is defined by

$$\alpha = \rho_\mathrm{m}/\rho_\mathrm{e}, \quad (2)$$

where ρ_m is the average molecular density. For the ideal gas, the temperature T is related to ρ_e by

$$T = P/(\rho_\mathrm{m} R) = P/(\alpha \rho_\mathrm{e} R), \quad (3)$$

where P is the pressure and R is the ideal gas constant. The self-sustaining flame system can be treated under the ideal gas law (Tieng *et al.*, 1992). It should be noted that the thermodynamic cycle of internal combustion engines is described by an Otto cycle, which is based on the ideal gas model.

In this study, we applied the CSI technique to an operating internal combustion engine and visualized the crank-angle dependency of Compton-scattered X-ray intensity at various positions inside the combustion chamber. We also attempted to estimate the crank-angle dependency of the gas temperature in the chamber.

2. Experiment

The time-resolved Compton-scattering imaging was performed at the High Energy Inelastic Scattering (BL08W) beamline (Sakurai, 1998) at SPring-8. The X-ray source is an elliptical multipole wiggler operated in the linear polarization mode (Maréchal *et al.*, 1998). The synchrotron radiation X-rays are monochromated and focused horizontally by an asymmetric Johann-type Si monochromator with (400) reflecting planes (Yamaoka *et al.*, 2000) to deliver 115.6 keV X-ray beams. A schematic of the experimental setup is illustrated in Fig. 1(*a*). The entrance slit system defined the size of the incident X-rays to 1 mm in both height and width. X-rays scattered from the gas inside the combustion chamber passed through a collimator with nine square apertures (1 mm × 1 mm each) arranged in a 3 × 3 array and were detected by the nine elements of a Ge solid-state detector (Ge-SSD). Therefore, the probing volume was approximately 1 mm^3. The intensity of the incident X-ray beams was monitored by an ion chamber for data normalization. The incident X-ray flux is estimated to be approximately 3×10^{12} photons s^{-1}.

A three-dimensional drawing of the compact model engine is shown in Fig. 1(*b*). The engine used in this study is a two-stroke engine with a displacement of 3.5 cc, manufactured by Enya Metal Products Co. Ltd. It has a cylinder bore diameter of 16.6 mm and a piston stroke length of 16.0 mm, resulting in a bore-to-stroke ratio close to 1. The combustion chamber volume is 306.79 mm^3, while the total cylinder volume is 3462.79 mm^3. In addition, since the volume when the exhaust port is closed is approximately 2400 mm^3, the compression ratio is about 8. The wall of the combustion chamber is made of an aluminium–silicon alloy with a thickness of 5 mm, and the X-ray transmittance at 115 keV is approximately 80%. This high transmittance ensures that the experiment can be performed without significant attenuation effects. The engine operates on a fuel mixture consisting of 90% methanol and 10% lubricating oil. The air–fuel mixture is formed at a stoichiometric air–fuel ratio of 6.4 or slightly lower and introduced into the engine. Fig. 1(*c*) shows a schematic diagram of the interior of the engine when the piston is at the bottom dead centre (BDC). The glow plug is heated to assist ignition only when the engine is started. At BDC, the intake port is open, allowing the air–fuel mixture to enter the combustion chamber. As the piston moves upward, the intake and exhaust ports close, and the mixture is compressed. At top dead centre (TDC), the compressed mixture ignites and burns, generating combustion pressure that drives the piston downward. As the piston descends, the exhaust port opens and the combustion gases are expelled. Further piston descent reopens the intake port, drawing in a fresh air–fuel mixture while expelling residual combustion gases through the exhaust port, completing the cycle. The engine operates through continuous repetition of these two processes – intake/compression and combustion/exhaust – driven by the reciprocating motion of the piston. In this experiment, the engine was operated at approximately 8000 to 9000 rpm. Measurements were conducted for one hour at each of seven locations in the horizontal direction inside the combustion chamber.

Fig. 1(*d*) shows a conceptual diagram of the time-resolved measurement. Signals from three Ge-SSD elements were recorded using TechnoAP's Digital Signal Processor (DSP) APN504X at channels CH1, CH2 and CH3, along with their respective acquisition times. Due to the limited number of DSP channels, only three of the nine elements of the Ge solid-state detector positioned directly above the incident X-ray beam were used. Additionally, signals from a non-contact rotational speed sensor (OH182/E), which generates signals when the piston reaches TDC and BDC, were recorded at CH4, along with their acquisition times. Based on the data acquisition time and the times at which the piston reaches TDC and BDC, it is possible to determine the piston position

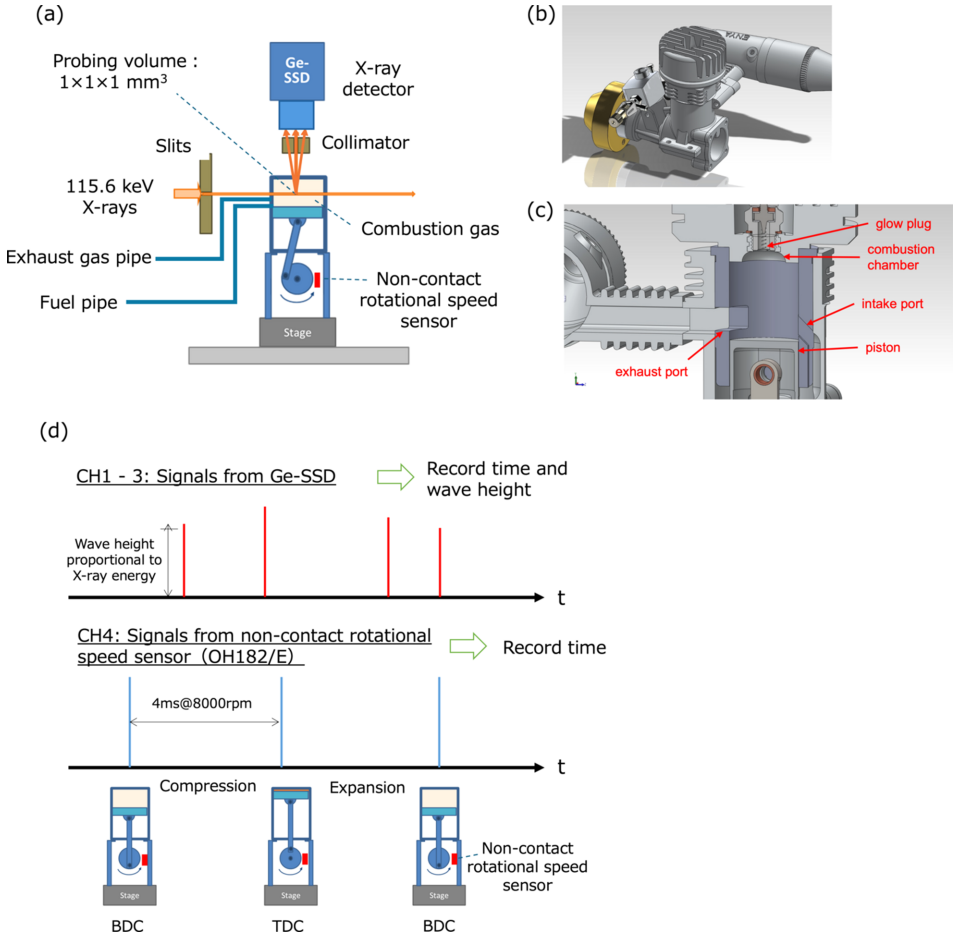

Figure 1
Schematic diagrams of the engine and experimental setup. (*a*) Schematic diagram of the experimental setup, (*b*) 3D drawing of the compact engine, (*c*) schematic diagram of the interior of the engine when the piston is at bottom dead centre (BDC) and (*d*) conceptual diagram of the time-resolved measurement.

at the moment of data acquisition. The travel time from BDC to TDC and that from TDC to BDC are each divided into 20 intervals, and signals within each time interval are accumulated, yielding spectra corresponding to 40 discretized piston positions (crank angles).

3. Results and discussion

To analyze the temporal evolution of the Compton-scattered X-ray spectra, the time from BDC to TDC and that from TDC to BDC were each divided into 20 segments, resulting in a total of 40 segments per cycle. The X-ray signals within each segment were accumulated, and by repeating this process for multiple cycles, the Compton-scattered X-ray spectra at piston positions (crank angles) were obtained. Fig. 2 shows the crank-angle-dependent X-ray spectra at the centre of the combustion chamber [P4 in Fig. 3(*a*)] during compression (crank angles $\theta = -180$ to $0°$) and expansion (crank angles $\theta = 0$–$180°$), where θ values of -175.5 and $4.5°$ correspond to the states at the onset of compression and expansion, respectively. Here, background X-rays were subtracted, as shown in the supporting information (Section S1) and the X-ray energy scale was converted to the electron momentum scale. The change in the spectra shows a gradual increase in intensity during compression and an abrupt decrease during expansion.

The crank-angle dependence of the integrated intensity of the Compton-scattered X-ray spectra at positions P1 to P7 in the combustion chamber, as shown in Fig. 3(*a*), is presented in Fig. 3(*b*). P4 represents the centre of the combustion chamber, while P1–P3 are located on the left side and P5–P7 on the right side at 1 mm intervals. For comparison, the intensities at positions other than P4 were scaled relative to the onset of intensity increase at P4, assuming that pre-combustion intensity changes are independent of position. During the compression process, the intensity begins to increase around a crank angle of $-100°$, when the exhaust port closes, and continues to rise until the piston reaches TDC (crank angle $0°$). After reaching TDC, the intensity starts to decrease and does so at a faster rate than during the compression process due to combustion. Around a crank angle of $120°$, the intake port opens and an increase in intensity associated with gas exchange is observed. Since the intensity of Compton-scattered X-rays reflects the electron density over the probing volume, its variation corresponds to the change of gas density associated with piston motion and combustion. Fig. 3(*c*) shows a two-dimensional map of the crank-angle dependency of the

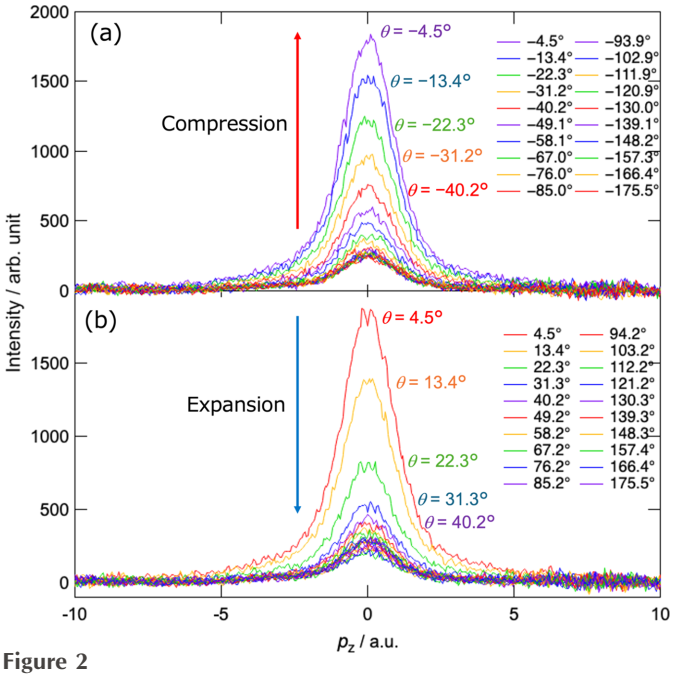

Figure 2
Time-resolved Compton-scattered X-ray spectra measured at the centre of the combustion chamber during piston motion. (*a*) Spectra divided into 20 intervals during the compression process from BDC (crank angle −180°) to TDC (crank angle 0°) and (*b*) spectra divided into 20 intervals during the expansion process from TDC (crank angle 0°) to BDC (crank angle 180°).

integrated intensity at P1–P7 before and after combustion, with intensity represented on a colour scale. The rate of intensity decrease is slower at positions farther from the centre of the combustion chamber. The rapid decrease in intensity due to combustion begins around a crank angle of 13.5° at positions P3–P6 located near the centre of the combustion chamber, whereas at positions farther from the centre the intensity decrease occurs slightly later, around a crank angle of 22.5°. In addition, the rate of intensity decrease becomes slower toward the outer regions. This behaviour is likely caused by a reduction in flame propagation speed due to a decrease in the velocity of turbulence near the walls, as well as a decrease in the mixture temperature resulting from heat exchange with the walls, leading to delayed combustion or the presence of unburned gas. Therefore, by time-resolved Compton-scattering measurements of the gas inside the combustion chamber of an operating engine, we successfully captured intensity changes corresponding to density variations associated with piston motion and gas combustion.

Pressure measurements in the combustion chamber were also conducted using the same type of model engine. This engine is equipped with a Kistler pressure sensor (type 6081A) to measure the pressure inside the combustion chamber. Fig. 4 shows a comparison between the crank-angle dependency of molecular density at P4 and pressure. Assuming that the molecular density is proportional to the Compton-scattering X-ray intensity, it is given by

$$\rho(\theta_{\rm CA}) = \rho_0 \frac{I(\theta_{\rm CA})}{I_0}, \qquad (4)$$

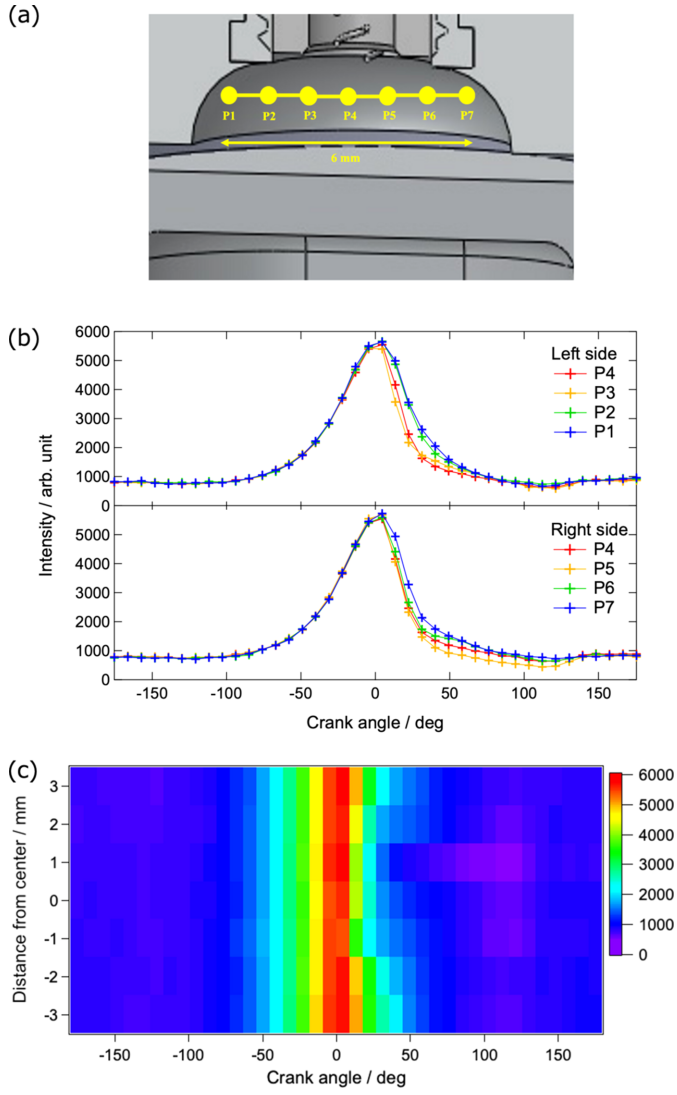

Figure 3
(*a*) Illustration of the interior of the combustion chamber, (*b*) crank-angle dependency of Compton-scattered X-ray intensities at positions P1–P7 and (*c*) corresponding two-dimensional map of the data shown in part (*b*). As illustrated in part (*a*), the measurement points in the combustion chamber, centred at P4 and spaced 1 mm apart, are indicated by yellow dots. On the vertical axis in part (*c*), P1 corresponds to −3 mm, P4 to 0 mm and P7 to 3 mm.

where $\theta_{\rm CA}$ is the crank angle, $\rho_0 = 2.5 \times 10^{25}\ {\rm m}^{-3}$ is the molecular density of the stoichiometric air–fuel mixture at 300 K and 1 bar, $I(\theta_{\rm CA})$ is the Compton-scattering X-ray intensity measured at a crank angle $\theta_{\rm CA}$ and I_0 is the Compton-scattering X-ray intensity at a crank angle $\theta_{\rm CA}$ of −175.5°. The pressure values shown are averages over 110 cycles at each crank angle, obtained while operating the model engine at a rotational speed of 8000 rpm. The pressure scale on the vertical axis is adjusted so that the rise in pressure coincides with the increase in the molecular density within the crank-angle range of −180 to −40°. The pressure increase during compression was more pronounced than the increase in the molecular density and the subsequent pressure drop occurred more gradually than the decrease in the density. This differ-

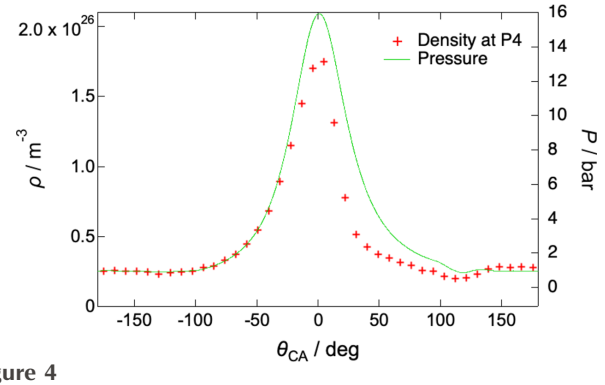

Figure 4
Comparison between the crank-angle dependency of molecular density at P4 and pressure. The red markers and green curve represent the molecular density and pressure, respectively. The pressure values shown are averages over 110 cycles at each crank angle, obtained while operating the model engine at a rotational speed of 8000 rpm. The molecular density is derived from the Compton-scattering X-ray intensity.

ence is attributed to the temperature increase during compression and combustion.

The gas temperature inside the combustion chamber can also be estimated using the Compton-scattered X-ray intensity and pressure. Assuming that the ideal gas equation of state holds, the temperature is proportional to the pressure divided by the X-ray intensity, as expressed by the following equation,

$$T(\theta_{\rm CA}) = T_0 \frac{P(\theta_{\rm CA})}{P_0} \frac{I_0}{I(\theta_{\rm CA})}, \quad (5)$$

where T_0 = 300 K is the temperature of the premixed air–fuel mixture before compression, $P(\theta_{\rm CA})$ is the pressure measured at a crank angle $\theta_{\rm CA}$ and P_0 is the pressure at a crank angle $\theta_{\rm CA}$ of −175.5°. Since the pressure and intensity values are known, the temperatures at other crank angles can be roughly estimated. At a crank angle of approximately −100°, the exhaust port closes and the gas is subsequently compressed, leading to a rise in temperature. Near TDC (crank angle 0°), the gas temperature reaches approximately 700 K, which is consistent with the temperature increase expected from adiabatic compression. In this engine, combustion is initiated by premixed compression ignition of methanol. The auto-ignition temperature of methanol is 737 K (National Fire Protection Association, 2010), which is expected to be exceeded near the glow plug when the piston reaches TDC. Combustion is completed at a crank angle of 31.3° and the temperature reaches a maximum of 1100 K. Around a crank angle of 120°, the intake port opens and the combustion gas is gradually replaced by a room-temperature air–fuel mixture, resulting in a decrease in temperature to 300 K. These results show the capability of Compton scattering for estimating the temperature of in-cylinder gases, together with pressure measurements.

It should be noted that the peak temperatures estimated in this study are lower than the temperature of static flames of propane around 1500 K (Sakurai *et al.*, 2016) and the adiabatic flame temperature of 2200 K for methanol (Haynes, 2015). This underestimation is most probably due to spatial and temporal averaging of the dynamically inhomogeneous gas temperature with the present experimental resolutions.

Finally, the temperature estimation in this work is based on the X-ray intensity analysis. An advanced analysis, such as the line-shape fitting, will improve the accuracy. A more detailed temperature evaluation based on model calculations is being conducted (Yamase *et al.*, 2026).

In conclusion, this article reports the first experiment of time-resolved Compton-scattering imaging with synchrotron-based high-energy X-rays on an operating internal combustion engine. The observed crank-angle dependency of Compton-scattered X-ray intensity allowed us to successfully capture the density changes of the gas in the combustion chamber associated with piston motion and combustion. Furthermore, by combining pressure measurements, the gas temperature in the combustion chamber of the operating engine was estimated successfully. This study demonstrates the capability of time-resolved Compton-scattering imaging as a unique technique to observe the dynamic behaviours of fuel and combustion gases in an internal combustion engine.

Acknowledgements

The authors thank Ken Enya (Enya Metal Products) for fruitful discussion about the model engine and for permission to use his drawings. We also thank Hiroshi Sakurai (Gunma University) for useful discussion concerning the data analysis and combustion. The Compton-scattering imaging experiment was performed with the approval of the Japan Synchrotron Radiation Research Institute (JASRI) (proposal Nos. 2022A1277, 2022B1176, 2023A1222 and 2023B1264).

Funding information

This work was supported by the Acquisition, Technology & Logistics Agency (ATLA) (project No. JPJ004596).

References

Bowditch, F. W. (1961). *A New Tool for Combustion Research – A Quartz Piston Engine*. SAE Technical Paper 610002. SAE, Warrendale, PA, USA.
Haynes, W. M. (2015). *Handbook of Chemistry and Physics*, 96th ed. CRC Press.
Itou, M., Orikasa, Y., Gogyo, Y., Suzuki, K., Sakurai, H., Uchimoto, Y. & Sakurai, Y. (2015). *J. Synchrotron Rad.* **22**, 161–164.
Maréchal, X.-M., Hara, T., Tanabe, T., Tanaka, T. & Kitamura, H. (1998). *J. Synchrotron Rad.* **5**, 431–433.
Miyazawa, T., Tsuji, N., Fujioka, D., Kaneko, T., Mizuno, Y., Uchimoto, Y., Imai, H. & Sakurai, Y. (2023). *Appl. Sci.* **13**, 10753.
National Fire Protection Association (2010). *Fire Protection Guide to Hazardous Materials*, 14th ed. Delmar Cengage Learning Press.
Sakurai, H., Kawahara, N., Itou, M., Tomita, E., Suzuki, K. & Sakurai, Y. (2016). *J. Synchrotron Rad.* **23**, 617–621.
Sakurai, H., Tsuji, N., Zama, Y., Suzuki, K., Hoshi, K., Hiramoto, D., Sakurai, Y. & Furuhata, T. (2021). *Crystals* **11**, 787.
Sakurai, Y. (1998). *J. Synchrotron Rad.* **5**, 208–214.
Sharaf, J. M. (2001). *Appl. Radiat. Isot.* **54**, 801–809.
Suzuki, K., Otsuka, Y., Tsuji, N., Hoshi, K., Sakurai, Y. & Sakurai, H. (2020). *Appl. Sci.* **10**, 5855.

Suzuki, K., Suzuki, S., Otsuka, Y., Tsuji, N., Jalkanen, K., Koskinen, J., Hoshi, K., Honkanen, A.-P., Hafiz, H., Sakurai, Y., Kanninen, M., Huotari, S., Bansil, A., Sakurai, H. & Barbiellini, B. (2021). *Appl. Phys. Lett.* **118**, 161902.

Tieng, S. M., Lai, W. Z. & Fujiwara, T. (1992). *Meas. Sci. Technol.* **3**, 1179–1187.

Tsuji, N., Tsuji, Y., Uchimoto, Y., Imai, H. & Sakurai, Y. (2021). *Appl. Sci.* **11**, 3851.

Yamaoka, H., Hiraoka, N., Ito, M., Mizumaki, M., Sakurai, Y., Kakutani, Y., Koizumi, A., Sakai, N. & Higashi, Y. (2000). *J. Synchrotron Rad.* **7**, 69–77.

Yamase, H., Mizuno, Y., Suzuki, H., Tsuji, N., Oguchi, T., Matsubara, G. & Sakurai, Y. (2026). In preparation.

Zhao, H. (2012). *Laser Diagnostics and Optical Measurement Techniques in Internal Combistion Engines.* SAE International Press.